Electronics and Electrical Engineering

AIMS Electronics and Electrical Engineering, 4(1): 87–113.
DOI: 10.3934/ElectrEng.2020.1.87
Received: 23 October 2019
Accepted: 14 December 2019
Published: 13 January 2020

http://www.aimspress.com/journal/ElectrEng

Review

Nanostructured metal oxide modification of a porous silicon interface for sensor applications: the question of water interaction, stability, platform diversity and sensitivity, and selectivity

James L. Gole*

School of Physics, Georgia Institute of Technology, Atlanta, Georgia, 30332, USA

*** Correspondence:** Email: james.gole@physics.gatech.edu; Tel: 404 874 9650.

Abstract: Key parameters of a nanostructure modified porous silicon (PSi) template that can affect the development and performance of PSi-based sensors are considered. The importance of pore selection and direct *in-situ* nitrogen functionalization are emphasized. Metal oxide nanostructured island sites deposited to select, well defined, and reproducible nano-pore walled, micron sized p and n-type silicon pores (0.7–1.5 μ diameter) provide enhanced selectivity. The micron-sized pores facilitate rapid Fickian analyte diffusion to these highly active sites. The metal oxide nanoparticles are trapped by a thin nanopored wall covering preventing their sintering at elevated temperatures. The varying sensitivities of the highly active metal oxide nanostructured sites are well predicted within the recently developed Inverse Hard/Soft Acid/Base (IHSAB) model. Nitrogen functionalization of the nanostructure decorated surfaces provides the conversion of these PSi interfaces from hydrophilic to hydrophobic character. The decrease of water interaction provides greatly enhanced stability. Selectivity can be extended to the measurement of multiple gases using a combination of nanostructured island site determined detection matrices, p and n-type charge carrier variation, time dependent diffusion response, and pore structure influenced sensitivity. The range of variable responses is dominated by the molecular electronic structure of the nanostructured island sites as evaluated using the IHSAB concept. Pulsed mode operation can facilitate low analyte consumption and high analyte selectivity and further provide the ability to assess false positive signals using Fast Fourier Transfer techniques. The modeling of the PSi sensor response with a new Fermi energy distribution –based response isotherm is found to be superior to other isotherms. The rate of sensor response, linearity of measurement, and hysteresis of response are also considered within the framework of the decorated micron sized pore structure.

Keywords: nanostructure driven electron transduction on porous silicon; hydrophobic sensor interfaces; stability; sensitivity; selectivity; IHSAB concept

Abbreviations: PSi: porous silicon; IHSAB: inverse hard/soft acid/base; UHP: ultra high purity; RH: relative humidity; FFT: fast Fourier transform; VOC: volatile organic compound; BTEX: benzene, toluene, ethylbenzene, xylene; FDF: Fermi distribution function; IV: product of current and voltage

1. Introduction

Sensors to detect noxious gases and vapors represent an ever-growing need in the current society [1]. In turn, this requires the development of new approaches, materials, and interfaces to improve sensor parameters [2,3]. Several studies have suggested that porous silicon (PSi) offers promise [2,3] as a useful man-made sensor material for the detection of gases and vapors with several advantages arising from the ability to adjust the size and location of pores (ex: nanometric to micrometric) [2–9] as one changes parameters of anodization (etch time, current density, wafer doping etc,) so as to produce a varied pore structure [1]. While it appears that PSi can be suitable for a diversity of gas and vapor sensors, including humidity sensors, the range of interfaces also results in distinct disadvantages entailed, in part, by arrays of pore structures that cannot be easily reproduced in various laboratories despite their formation under similar silicon porosification [10]. A range of viable solutions to this drawback can be provided by a specific and readily reproducible micrometric pore structure whose response is regulated by metal oxide nanoparticle island (10–30 μ) sites deposited to the PSi interface and stabilized by direct in-situ nitridation. This has multiple effects.

Porous semiconductor sensors are, in general, highly selective to water vapor, organic solvents, and oxidizing gases such as NO_2 and O_3. We will suggest that potential solutions to this problem [11] are obtained by creating hydrophobic surfaces with open micron sized pore structures. Further, it appears possible to not only reduce noted water and organic solvent surface interactions [1,12] but also to transform oxidized PSi surfaces through direct nitration so as to introduce enhanced stability. The slow response of many PSi devices [1,12] due to limited mass transport and capillary condensation can also be overcome using open 0.7–1.5 micron sized pores. This structure also appears to reduce hysteresis [13,14]. A loss in sensitivity can be overcome by introducing highly active metal oxide nanostructured island sites to these pores. Linearity [15], a problem with many semiconductor-based devices, can be partially compensated by evaluating the first and second derivatives of the sensor response. A bewildering irreducibility of pore size has been observed for both mesoporous and microporous PSi, as samples prepared in several laboratories [4,6,8–10,16] differ even if a similar technological process of silicon porosification is used. This places emphasis on the need to carefully and closely monitor not only the etch parameters of a specific established etch procedure but also the precise placement of those samples to be etched to effect reproducibility. This can be accomplished if one takes advantage of micron (0.7–1.5 μ) sized pore generation [17]. As we will outline, the analysis of false positive sensing on the porous silicon interface can be accomplished with pulsing techniques borrowed from acoustic theory [19]. All semiconductor devices suffer from low selectivity. At this point it is possible to monitor two and sometimes three gases simultaneously with potential extension to additional gases with an array-based format relying on the combination of p and n-type silicon doping in concert with metal oxide nanostructure modified sensor interfaces [20–23].

The PSi based sensor platform design including sensor fabrication, nanostructure deposition, and gas detection, which we review in this study have been described in detail elsewhere [17,24–31].The basic semiconductor interface is illustrated in Figure 1. This structure, used in the studies outlined here,

is produced by a hybrid etch procedure to create an interfacial porous silicon support structure. As Figure 1 indicates, nanopore (thin film-green) covered micropores, created specifically to facilitate efficient gaseous Fickian diffusion [17,29] to the highly active nanoparticle (red) modified nanopore (green) wall coating. The active nanoparticle island sites can be chosen from a selection of metal oxides including TiO_2, SnO_x, NiO, Cu_xO, and Au_xO (x >> 1, decreasing in the Lewis acidity of the metal oxide sites. These island sites control an electron transduction process as the reversible interaction of select analytes with the metal oxide decorated PSi interface is well represented by the recently developed IHSAB model. Highly accurate repeat depositions are not required as the island sites are deposited at sufficiently low concentration so as not to interact electronically with each other. Varied nanostructured metal oxide sites produce a matrix of easily detected sensor responses that form a basis for changing the sensitivity to specific analyte gases. This exposure alters the interface conductivity to the gold contacts shown in Figure 1. Operated in the electron transduction mode, the transfer of electrons to an n-type PS interface, as would occur with a basic analyte, increases the majority charge carriers which are electrons, decreases conductmetric resistance, and increases conductance. The removal of electrons, as would occur with an acidic analyte, decreases the majority charge carrier concentration and the conductance and increases resistance.

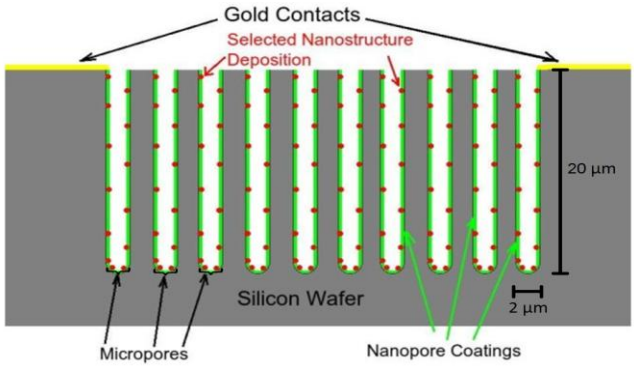

Figure 1. Schematic representation of PS sensor platform [34]. Elsevier by permission.

The opposite behavior will be observed for a p-type semiconductor interface. For the n-type and p-type systems, the micropores are respectively ~0.7 to 1 µm and 0.8 to 1.5 µm in diameter. The reversible interaction of select analytes with the metal oxide decorated PSi interface is well represented by the recently developed IHSAB model [32].

2. A desired pore structure, platform, and sensor response

We suggest that it is possible to focus on a single, well established, and reproducible pore structure as an efficient analyte trapping template. The selected pore structure described in Figure 1, with its attendant nanostructure deposition, is exemplified in Figures 2 and 3 [32–34]. Note that the nanoparticle deposition does not require time consuming and costly self-assembly or costly and time-intensive lithographic assembly. The nanostructured island sites, once deposited to the interface, are sustained on that interface in the size range 10–30 nm with no evidence for sintering with increased temperature. We require only that the concentration of the nanostructures be maintained at a level so as to avoid cross talk between these structures which will degrade the conductometric response of the interface. In other words, there is an optimum deposition concentration for each nanostructure deposition. However, the deposition process requires no additional control and does not demand that

the nanostructured islands be placed precisely at the same points in the micropores. This simplicity of design follows a process that is much more energy efficient than is thin or thick film design and provides reproducible sensing. Counter to traditional metal oxide systems [35–46], dispersed metal oxides on PSi do not require operation at high temperature. Therefore, they are more energy efficient and respond more rapidly due to their dispersed nature. Room temperature operative design, adds considerable flexibility not possible in a singly or multiply "coated" metal oxide interface.

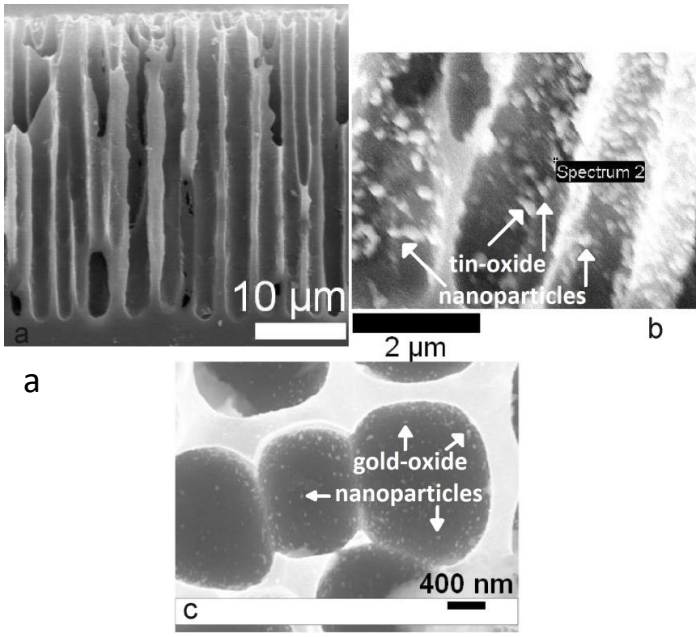

Figure 2. (a) Close up side view of hybrid porous silicon film. (b) Nanoparticle tin-oxide coating on porous silicon micropores; (c) 10 to 30 nm Au_xO nanostructures on porous silicon. From J. L. Gole and S. Ozdemir (Gole and Ozdemir, ChemPhysChem, 11, 2573–2581 (2010) Wiley by permission. Copyright © 2010 WILEY-VCH Verlag GmbH & Co. KGaA, Weinheim.

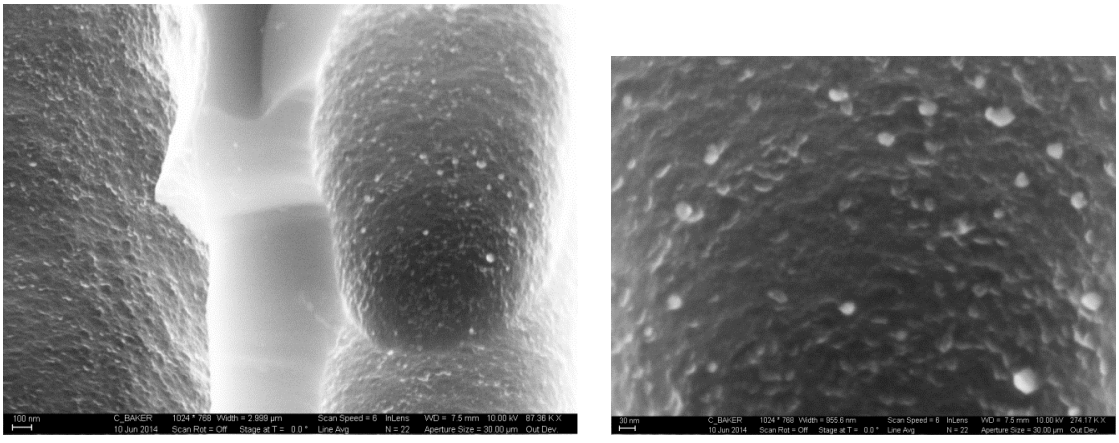

(a) (b)

Figure 3. (a) SEM image of thiol treated TiO_2 decorated porous silicon at 87.36 KX magnification (b) SEM image of thiol treated TiO_2 decorated porous silicon at 274.17 KX magnification. The lighter images in the micrographs correspond to sulphur-based moiety functionalized titanium oxide [34]. Elsevier by permission.

As metal oxide sensors need to operate at elevated temperatures [36,44–46], a power consuming heating element must be provided with the sensor housing. In several applications it is necessary to tightly control the temperature of the sensor element as it is intimately tied to the correct identification of the gas of interest.

Distinguishing one gas from another requires that the heating element and sensor be well-separated (channel) from the remaining electronics. This means that the sensor configuration can be greatly affected by an impinging combustion or flue gas, rendering difficult the correct identification of gaseous species in the flow. The PSi sensor configuration depicted in Figure 1 consumes less power as it does not require the complexity of a system separated sensor/heater configuration. In contrast to traditional metal oxide systems, this PSi device can be extended in a heat sunk configuration to probe elevated temperature environments. This suggests that it might be used to monitor high temperature flue gas flows [17,47].

Representative sensor responses are depicted in Figures 4–6. Figure 4 depicts the response for PH_3 for a p-type PSi interface. This response is very similar to that observed for NH_3. Figure 5 depicts the response for NO_2 on a p-type PSi interface. In contrast, Figure 6 depicts the responses for NH_3, and NO_2 on an n-type interface. This figure also includes comparative results for NO. Typical responses, which can be used to form response matrices, are presented in Tables 1 and 2.

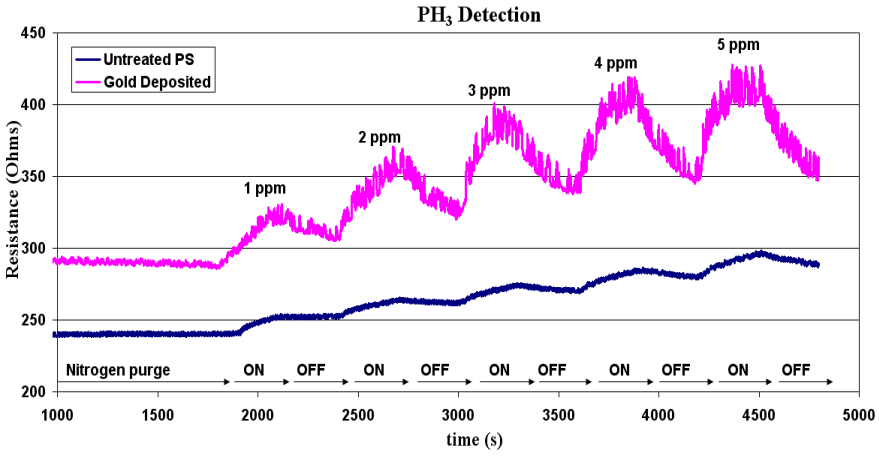

Figure 4. Improved response of a basic analyte, PH_3, to a p-type PS sensor with an electroless Au_xO deposit. Here, 1, 2, 3, 4, and 5 ppm of PH_3 is pulsed onto the sensor surface every 300 s. A p-type sensor is used as the gold clustered oxide deposition enhances the response of the un-treated porous silicon interface by a factor of five. Reprinted from J. L. Gole, S. Ozdemir, Nanostructure Directed Physisorption vs.Chemisorption at Semiconductor Interfaces: The Inverse of the Hard-Soft Acid-Base (HSAB) Concept, Chem. Phys. Chem. 11, 2573–2581, 2010, Wiley by permission. Copyright © 2010 WILEY-VCH Verlag GmbH & Co. KGaA, Weinheim.

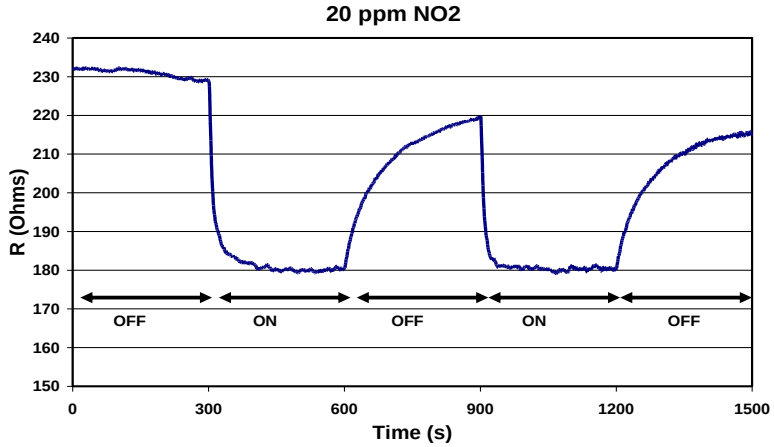

Figure 5. Response of an acidic analyte, NO_2, to a p-type PS sensor. Conductivity increases upon exposure to the moderate acid. The return to baseline is not complete at this concentration as NO_2 sticks to the surface in this open experimental configuration. From S. Ozdemir, T. Osburn, J. L. Gole, Nanostructure Modified Gas Sensor Detection Matrix for NO Transient Conversion of NO to NO_2, Journal of the Electrochemical Society. 158 (2011) J201-J207. ECS by permission.

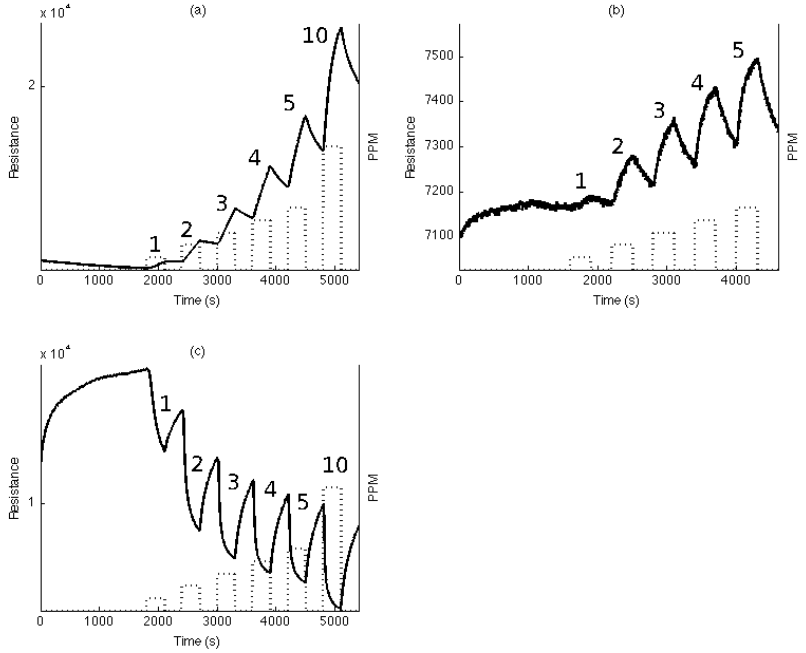

Figure 6. Resistance response of n-type porous silicon sensors to 1–5 ppm and 10 ppm of (a) NO_2, (b) NO and (c) NH_3. NO_2 acts as a moderate acid, NO as a weak acid (resistance increase), and NH_3 as a strong base (conductance increase). Compare the results for NH_3 to those for PH_3 (Figure 4). From S. Ozdemir, T. Osburn, J. L. Gole, Nanostructure Modified Gas Sensor Detection Matrix for NO Transient Conversion of NO to NO_2, Journal of the Electrochemical Society. 158, J201-J207.2011. ECS by permission.

Table 1. Relative increase in response (increase in resistance) of SnO_2, NiO, Cu_xO, and gold clustered oxide, Au_xO treated "p-type" PS interfaces relative to the untreated interface. The table constitutes a response matrix to the gases PH_3, NO, NH_3, and SO_2. From J. L. Gole and S. Ozdemir ChemPhysChem, 11, 2573–2581 2010. Wiley by permission. Copyright © 2010 WILEY-VCH Verlag GmbH & Co. KGaA, Weinheim.

	SnO_2	NiO	Cu_xO	Au_xO
PH_3	2	2.5	4	5
NO	7–10	3.5	1	1.5–2
NH_3	1.5	1.5–2	2-2.5	~3
SO_2	4	(2)	1+	2

Table 2. Relative increase or decrease in resistance (decrease or increase in conductance) of TiO_2, SnO_x, NiO, Cu_xO, and gold clustered oxide, Au_xO treated "n-type" PSi interfaces. The table constitutes a response matrix for the gases NO, NO_2, and NH_3.

	TiO_2	SnO_2	NiO	Cu_xO	Au_xO
NO	-12*	-2*	4	1.2	1.5–2
NO_2	0.75	0.5**	(0.9–1)	1	1.5–2**
NH_3*	-(3.5–4)	-2.5	-1.5	-2	-3
PH_3	2–2.5				

*Note: Indicates decrease in resistance with analyte exposure and increase in conductance

Note: Indicates initial response, From Gole J. L., Goude E. C., Laminack W. (2012) Chem. Phys. Chem: **13: 549–561. Wiley by permission. Copyright © 2012 WILEY-VCH Verlag GmbH & Co. KGaA, Weinheim.

2.1. Sensor responses and the IHSAB model

The exemplified response data has been used to develop a general model applied to obtain the sensor responses that we have outlined. We combine the properties of both p and n-type extrinsic semiconductors with a molecular orbital model for the interaction of the nanostructured metal oxides to demonstrate the coupling of the nanostructure response to the semiconductor majority charge carriers. An analyte can donate electrons to a "p-type" porous silicon semiconductor and these electrons combine with holes, thus reducing the number of majority charge carriers. This leads to an increased interface resistance (decreased conductance). The process is reversed for an "n-type" semiconductor as the majority charge carriers, electrons, increase and the resistance decreases (increased conductance). Basic analytes donate electrons whereas acidic analytes accept electrons, however, this process can be influenced by the acid strength of the nanostructured metal oxides introduced to the porous silicon interface. Within this framework sensor system sensitivities and reversibility can be predicted from the recently developed Inverse Hard/Soft Acid/Base (IHSAB) model [14,17,26,32,34,47,48], which provides a means of linking chemical selectivity and the mechanism of sensor response. This model combines the basic tenants of acid/base chemistry (the ability of bases to donate electrons and acids to seek electrons) and semiconductor physics. The materials selected for nanostructured island sites serve the role of guiding gateways to force a dominant electron transduction (vs. chemisorption) at the decorated extrinsic semiconductor interface. The selection of these nanostructures and the variable and controllable reversible interaction they introduce

for sensor applications is well predicted by the IHSAB model as it dictates the coupling of analyte/interface acid-base interactions with the properties of the majority carriers in an extrinsic semiconductor. The inverse hard and soft acid and base (IHSAB) concept [14,17,26,32,34,47] complements the tenants of HSAB interactions [48].

The properties of acids and bases can be described as hard and soft based upon the correlation of several atomic/molecular properties that include the ionization potential, the electron affinity, and the chemical potential. These can be correlated with the highest occupied molecular orbital (HOMO) – lowest unoccupied molecular orbital (LUMO) gap concept from molecular orbital theory [31]. For a soft acid, the acceptor atom is of low positive charge, of large size, and has polarizable outer electrons. In a hard acid the acceptor atom is of small size and not easily polarized. In a soft base the donor atom is of low electronegativity. It is easily oxidized and highly polarizable with low-lying unoccupied molecular orbitals. The concept of hardness reduces to the statement: hard molecules have a large HOMO-LUMO gap and soft molecules have a small HOMO-LUMO gap [17]. The IHSAB principle focuses on a HOMO-LUMO mismatch to minimize chemisorption and induce the efficient transfer of electrons.

Based on the reversible interaction of hard acids and bases with soft bases and acids, the IHSAB principle enables the selection of interacting materials that do not form strong covalent or ionic chemical bonds. Thus it represents the inverse of the HSAB model [49,50] for significant bond formation based on strong ionic (hard acid/base) or covalent (soft acid/base) interactions and chemical bond formation. The selection of metal oxide nanostructures that are deposited to nanopore covered microchannels can be predicated based on a clearly designed procedure and established materials properties.

Estimated positions of hard through soft deposited nanostructures and gas analytes on the IHSAB scale are shown relative to PSi in Figure 7. The relative positions in this Materials Table are dictated by the observed interactions of the indicated analytes (lower portion of the figure) and the nanostructured metal oxides (upper scale). As dictated by the IHSAB model, the porous silicon (PSi) interface deposited with Au_xO nanostructures will produce the largest response to NH_3, with which it has the largest mismatch, and the PSi deposited with TiO_2 will produce the largest response to CO. Within the IHSAB framework, metal oxide nanostructure depositions can be selected for the PSi sensor interface to create a predictable range of sensitivities for various gases. The relative responses observed for select n-type and p-type PS interfaces allow the construction of the "Materials Positioning Table" for the acids and bases within the IHSAB concept. The analyte response data forms the basis for the development of the materials positioning diagram, based largely on the interaction of the acidic metal oxides ranging from TiO_2 to Au_xO ($x >> 1$) and the bases from NH_3 to CO.

The basis for positioning H_2S, NO_2, NO, and PH_3 is their responses relative to an untreated porous silicon interface as exemplified in Tables 1–3. Responses for NO_2 are discussed elsewhere [26–28]. The data for H_2S is exemplary. Here TiO_2 nanostructures on the PSi interface greatly improve the response of the decorated interface [23]. This is the result of the significant mismatch with the strong acid TiO_2.The mismatch and relative sensor response for SnO_2 decrease but are still significantly higher than PSi. Nickel oxide nanostructures are very closely matched with H_2S and hardly change the sensor response relative to the PSi interface [29]. Similar results are obtained with Cu_xO, largely in response to CuO for all the gases considered. This suggests that NiO and Cu_xO are rather poor sensors for H_2S. However, the data in Table 3 demonstrates a substantial upturn for Au_xO nanostructure depositions and a very significant increase in this weak acid decorated sensor response compared to the PSi interface. All of the responses in Tables 1–3 demonstrate a clear dependence of the sensor response on "strong acid"- "weak base" or "weak acid"- "strong base"

interactions which produce an orbital mismatch leading to a significant sensor response. However, the observed dependence, which complements reactive interaction, in many instances shows a parabolic dependence whose minimum lies at NiO and Cu_xO corresponding to these notably reactive metal oxide structures.

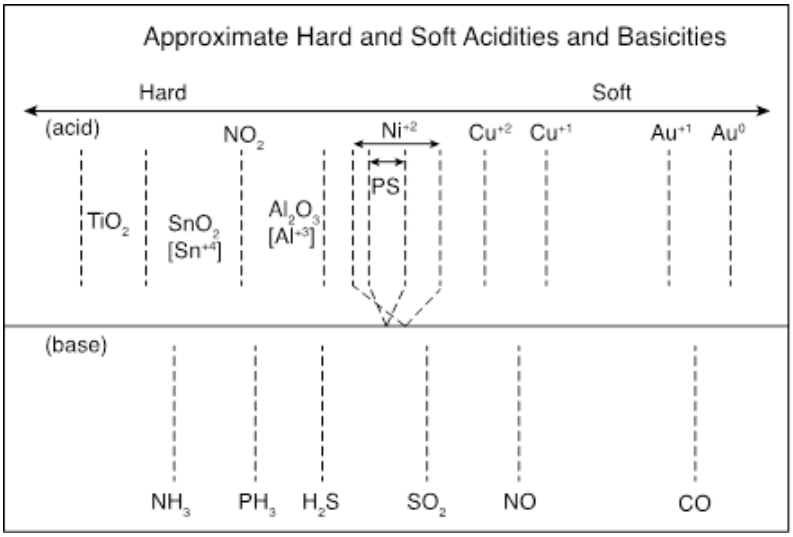

Figure 7. Estimated hard and soft acidities and basicities based on resistance changes relative to a p-type and n- type porous silicon interface. The acidic metal oxides that decorate the semiconductor interface can be modified [24,54] . The analytes remain as positioned. A horizontal line is used to separate the metal oxides used to modify the PSi interface (above) and the analytes below in the figure.

Table 3. ΔR(deposited)/ΔR(untreated) values are shown for H_2S impedance changes on p-type extrinsic semiconductor interfaces. Comparison is to an uncoated p-type PS sensor. The nanostructured deposits to the PS surface are indicated in the Table. Base resistance of the sensors used in these experiments varied from 300 to 600 Ω. From C. Baker, W. Laminack, and J. L. Gole [30], Sens. Actuators B Chem, 212, 28–34, 2015.

	PS substrate	TiO_2	SnO_2	NiO	Au_xO
H_2S	1	60	22	2	1200

3. Reducing interference from humidity, enhancing stability

3.1. Pore diameter induced hydrophobicity

High sensitivity to air humidity is known to lead to instability in PSi-based gas sensing parameters [51–53] making it difficult to distinguish between humidity and gas concentration. Schecter et al. [54] suggested the creation of a hydrophobic surface on PSi as hydrophilic regions absorb polar water molecules through hydrogen bonding and hydrophobic regions, as obtained in freshly prepared PSi, display very weak dispersion forces and do not absorb water. Schecter demonstrated that water vapor affected the conductivity of hydrophobic PSi only at a high humidity level and after prolonged exposure [55]. However, the oxidation of PSi during storage creates hydrophilic regions (ex. silicon oxides) and requires the restoration of hydrophobic character through

additional electrochemical treatment, restoration in a hydrogen atmosphere [56], or storage under UHP nitrogen. Alternately [57,58], the PSi surface might be modified by depositing a monolayer of a hydrophobic agent, usually a polymer. However, thin films can change the surface porosity and chemical resistance and may suffer long- term interaction with water vapor. Further, polymer coatings are generally not amenable to even moderate increases in temperature [1]. Pore size selection and subsequent nitridation offer a more acceptable, efficient approach.

In addition to the hydrophobic character of PSi-based interfaces, pore size selection and reproducibility can represent extremely important parameters. The Kelvin equation [59] predicts that water vapor begins to condense at room temperature and 15% relative humidity for pore sizes of order 2 nm [1]. At a relative humidity of ~ 90–100%, capillary condensation occurs for pores of ~100 nm diameter [1]. PSi with a pore size in the range 2–10 nm is optimal for measuring humidity in the low RH range while PSi with pores in the range 20–100 nm is preferable for developing humidity sensors. Sensors with the larger pore size have low sensitivity at low water concentration and begin to show increased sensitivity only at RH values exceeding 60–80%. The selected micron pore diameters emphasized in the present study range from 700 to 1500 nm. This suggests a negligible sensitivity to water vapor which weighs heavily on long term stability and presents a pore size induced longer-term stability. This has been observed repeatedly. The micron sized pores are also found to result in a minimal sensitivity to organic solvent vapors and volatile organic compounds [24].

3.2. Direct nitridation,induced hydrophobicity, and long term stability

Recently, the process of direct *in-situ* nitridation has been applied to the ready conversion of TiO_2 nanocolloids to visible light absorbing $TiO_{2-x}N_x$ [60,61]. This approach has been extended to the nitridation of the nanostructured metal oxide deposited PSi interfaces, tuning the response of the reversibly interacting sensor sites [29,62]. Recent studies by Wang et al. [63] have demonstrated the visible light driven reversible and switchable hydrophobic to hydrophilic conversion of titanium oxynitride nanorods. These strongly hydrophobic nanorods which were approximately 135 nm in length and 35 nm in diameter (vs. the 10 to 30 nm PSi island site deposits) demonstrated contact angles as high as 141 º. Their transformation under visible light illumination can be reversed from hydrophilic to hydrophobic character with moderate 120 ℃ sintering or ~2 week storage in a dark environment. The importance of this study is that it demonstrates the ready transformation for the nanorod treated surface. By comparison, the analyte responses shown in Figures 8 and 9 indicate the ready direct nitridaton of the PSi interface. A more efficient and rapid nitration of the subsequent metal oxide nanostructured deposits is observed [62].

Figure 8 corresponds to the responses observed when NH_3 contributes electrons to an untreated and nitridated n-type PSi interface. Here, the PSi interface is treated for 15 seconds with triethylamine. This is a much shorter time scale then that required to produce the titanium oxynitride nanorods [63]. The interaction of NH_3 contributes electrons and increases the majority charge carrier concentration (electrons) and the conductance for both the nitridated and the untreated PSi interfaces. However, the conductance increase (response) is considerably greater for the nitridated interface. The nitridation process enhances the basicity (decreases the Lewis acidity) of the PSi surface corresponding to a shift toward the soft acid side of Figure 7. The HOMO (donor)-LUMO (accepter) orbital mismatch increases for the nitridated PSi and its interaction with NH_3. The IHSAB principle thus predicts the increased response after nitridation. The nitridation of the metal oxide nanostructured island sites is equally if not more efficient [29,62]. Figure 9 demonstrates that the

nitridation process extended to one hour produces a similar, if not more pronounced, modification of the PSi interface response. One observes a more rapid rise in system response as well as the signal decay as the gas flow is removed. The efficiency of the nitridation process relative to that of the $TiO_{2-x}N_x$ nanorods suggests a ready approach to nitridation of the decorated PSi interface to produce a high degree of hydrophobicity and thus enhance long-term stability**.**

The further importance of the nitridation process has been highlighted in recent studies of silicon oxynitride films, the preparation, performance, and application of which have recently been reviewed [64]. In contrast to the degradation and stability issues associated with PSi thin film sensors and the difficulty entailed in their use in standard CMOS circuits or flexible substrates, SiO_xN_y films are found to offer several distinct advantages associated with the nitridation process. Using a variety of film preparation methods, the oxynitride preparation process usually involves the reaction of N_2O, NO, NH_3, or N_2 with SiO_2 or O_2 with Si_3N_4 under suitable conditions to obtain variable SiO_xN_y films [64]. This is exemplified as one uses high temperature nitridation processes. For example, the introduction of nitrogen to an SiO_2 film by thermal nitriding [65], rapid annealing [66], and plasma nitriding [67], under certain precisely controlled conditions. All of these processes have their advantages and disadvantages. However, as they are more formation applied, they are found to produce stable SiO_xN_y films which show promise for optical devices with tunable refractive indices and scratch resistant coatings among other applications [64]. The results obtained for SiO_xN_y films emphasize the importance and diversity of the nitridation process in the formation of the oxynitride, as well as the stability that it introduces. By comparison, the process of nitriding the untreated and metal oxide decorated micron pored PSi interface can be applied, producing an oxynitride-based interface and efficiently introducing hydrophobic character. It should be clear that the amine-based nitridation process is best applied immediately after pore formation and subsequent metal oxide nanostructure deposition. The rapid oxidation of the nanostructured metal oxide island sites is desirable and adds efficiency to the nitration of the porous silicon template.

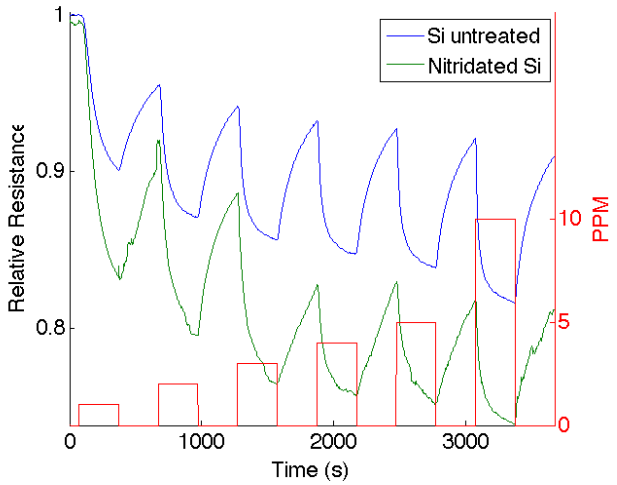

Figure 8. Response of an untreated PS interface to NH_3 (blue) and after nitridation of the interface for 15 seconds with triethylamine (green). The boxes (red) denote the analyte concentration from 1 to 10 ppm from the beginning of the gas introduction to the end. A rapid response is observed at each concentration. Nitridation produces an increase in the interface response as monitored as an increase in conductance (decrease in resistance).

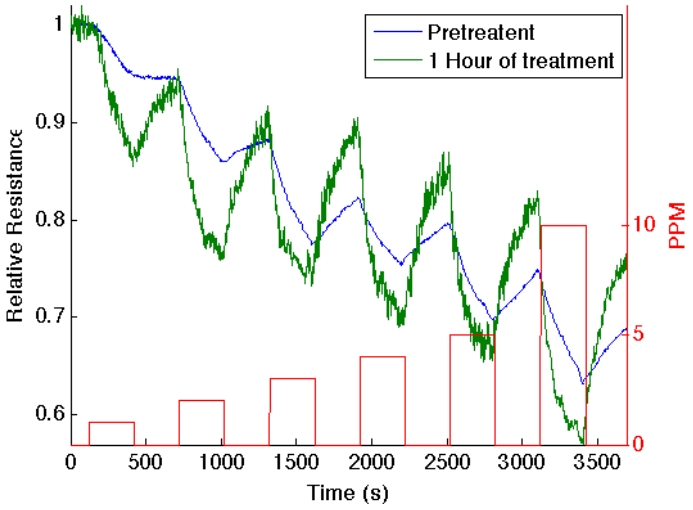

Figure 9. Response of an untreated PS interface to NH_3 (blue) and after nitridation of the interface for one hour with triethylamine (green). The boxes (red) denote the analyte concentration from 1 to 10 ppm from the beginning of the gas introduction to the end. A rapid response is observed at each concentration. Nitridation produces an increase in the interface response as monitored as an increase in conductance (decrease in resistance).

Oxidation introduces further hydrophilicity to the PSi interface through exposure to the weak Si-Si bond. Further, SiO_2 formation can be facilitated through interaction with strongly oxidizing analytes including NO_2 and O_3 (weak O-O_2 bond [68]). However, the observed efficiency with which the silicon oxynitrides can be formed upon nitridation of SiO_2 and the enhanced interaction of the alkyl amines for in-situ nitridation should obviate this problem.

In summary, the interaction of a micrometric open pore structure can offer an efficient means of greatly eliminating or at least minimizing the interference of water in PSi sensor applications. The use of PSi as a template for metal oxide nanostructured island sites and the subsequent nitridation of this interface provides a means of transforming the interface to hydrophobic verses hydrophilic character, further reducing water vapor interaction. These approaches greatly diminish sensor degradation and enhance longer-term stability.

3.3. Driving off water with moderate temperature heating of a heat sunk configuration

In contrast to traditional metal oxide sensors, the configuration of the decorated PSi interface, which we have outlined, also can lend itself to water elimination through limited heating using a heat sunk configuration [17]. Figure 10 indicates responses [30] for an Au_xO (x >> 1) nanostructure decorated p-type PSi interface for H_2S analyte concentrations of 6, 12,18, 24, 30, and 60 ppm in a nitrogen carrier gas [30]. These responses are significantly greater than that for an untreated p-type interface (Table 3). The substantial enhancement of the response after Au_xO decoration indicates that this acid lies far to the weak acid side of H_2S in Figure 7 and displays a significant orbital mismatch with the sulfurous base. Figure 11 indicates [30] the response of this system after the decorated silicon interface is exposed to extremely high humidity (~80% RH) for an extended period. It should be clear that the response is much lower than that in Figure 10 indicating the quenching of the response signal due to water vapor interference. We compare the response of the same sensor heated to 50 ℃ for 20 minutes before retesting. The subsequent signal enhancement indicates that the sensor

can be partially rejuvenated. The rejuvenation process appears to be more effective at low analyte concentrations in this highly humid environment. Because this mode of water removal is simple, the temperature is easily accessible through a simple heat sunk device, and the heater can be operated for extended periods with little device damage, this approach appears promising.

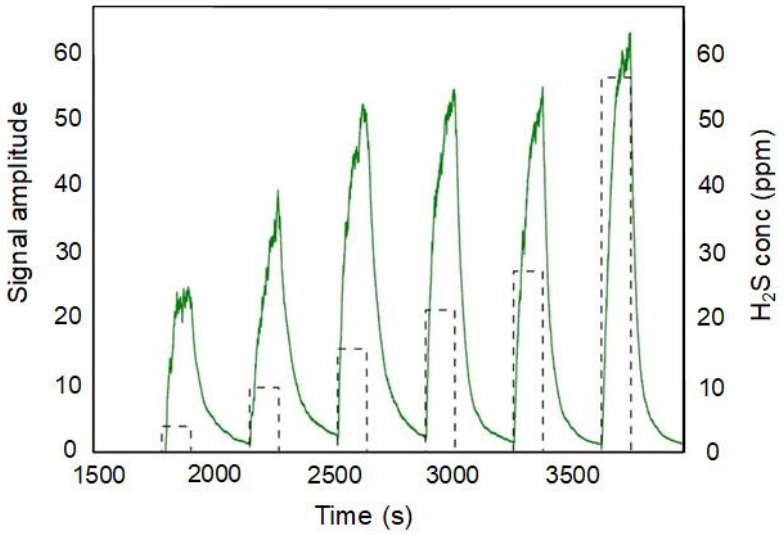

Figure 10. Response of an untreated (blue) and Au_xO treated porous silicon (PSi) interface to H_2S.The PSi interface was exposed to Au_xO for 15 seconds. The black dashed boxes denote the analyte concentration over the time of sensor exposure. The response at each concentration is rapid as is the recovery leading to a nearly constant baseline [30].

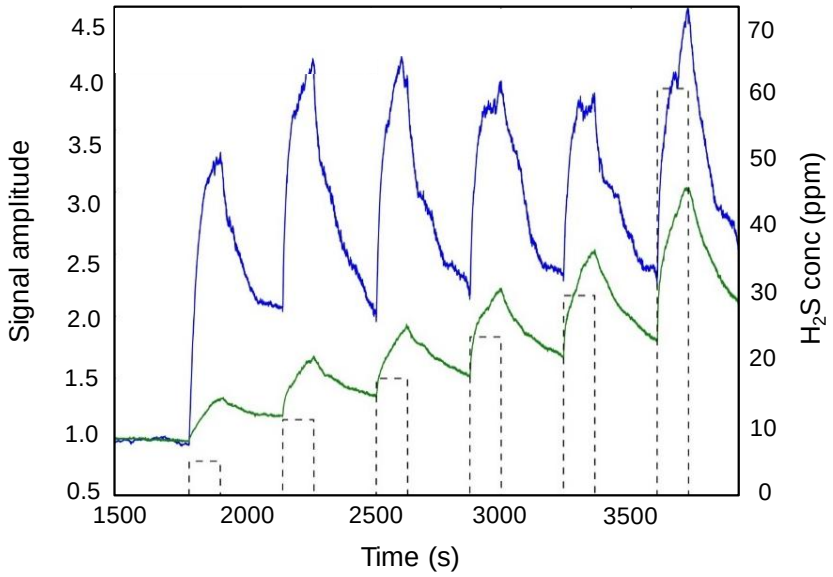

Figure 11. Response of an Au_xO treated porous silicon (PSi) interface (green) to H_2S, after exposure to substantial humidity and its comparison to the same Au_xO treated interface after 20 minutes of heating at 50 ℃ (blue). The PS interface was exposed to Au_xO for 15 seconds. A rapid initial response is observed at each concentration whereas the heated PSi sensor at first displays a considerably enhanced response, which again shows some quenching at concentrations of 24, 30, and 60 ppm. The black dashed boxes denote the analyte concentration from 6 to 60 ppm over the indicated time range [30].

4. Linearity of response and hysteresis

By greatly reducing, if not obviating, the effect of humidity sensitivity, select micron pored PSi (Figure 1) can improve the linearity of sensor response and decrease hysteresis. In concert, direct nitridation of those nanostructured metal oxide island sites deposited to the PSi interface greatly enhances their hydrophobic character. Significant changes induced by the interaction and condensation of water and by organic solvent vapor can be greatly mitigated.

Alternately, for conductometric measurements, the time derivative of the sensor signal can be shown to be linear as it largely reflects the onset of the response at a given analyte concentration and despite signal quenching at higher concentrations. The amplitude of the spikes (Figure 12) in the first derivative of the sensor response at low concentration correlates closely and nearly linearly with the ambient gas concentration. These first derivatives are advantageous in that they spike early in the gas pulse, long before the sensor reaches saturation.This allows for the quick evaluation of a response. Using the information gleaned from this simple evaluation, it is possible to extract gas concentrations from the sensor responses [21,23] as exemplified in Figure 12.

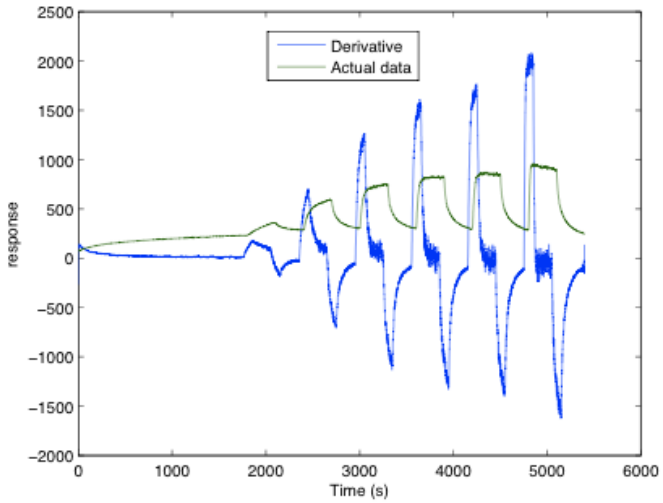

Figure 12. Conductometric response for NO on Au_xO treated n-type PS and its time derivative. Note the quick response to the analyte gas seen in the time derivatives and observe that they increase nearly linearly with gas concentration at low ppm. W. Laminack, C. Baker, and J. L. Gole, ECS Transactions, Vol 69**,** 2, pp. 141–152, 2015. ECS by permission.

Figure 13 shows the normalized resistance response to NO on "n-type" PSi, corresponding to the resistance change of a sensor in the presence of analyte gas, divided by the baseline response. The average response in Figure 13 is over several different sensors with distinctly different coatings. All have a similar response, as a function of concentration, which is also found to be similar to the PH_3 response on "p+-type" sensors [69]. The response is near linear at very low ppm concentrations (1 ppm to 4 ppm), however, it begins to saturate at higher concentrations. The non-linearity of the response at higher concentrations complicates the use of the raw response data to find the analyte gas concentration. Because the sensors can require an extended time to reach their saturated response, dependent upon the nature of the analyte gas, measurements are taken in an unsaturated mode [48].The derivative of the sensor response quickly determines the approximate concentration of the gas, as the maximum size of the spike in the derivative correlates nearly linearly with the

concentration of the analyte gas. The spike in the derivative appears almost instantaneously once the gas interacts with the PS surface; however, the spike quickly tapers off until the gas concentration is changed. Although taking the time derivative of the simulated conductometric response is straightforward, the raw sensor data can display noise that can cause spurious signals in the derivative. In order to remove the noise, a moving average has been used [20,70,71]. This moving average takes some previous number of points and averages over these points to smooth over the derivatives.

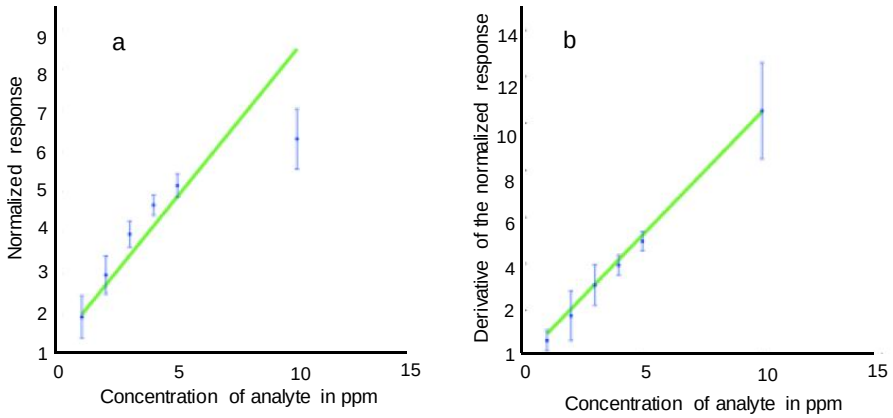

Figure 13. Normalized response (left) to NO for several different n-type sensors and the magnitude of the first derivatives (right) of the normalized response. Blue points are actual data (with error bars) and the green line is the linear fit. W. Laminack, C. Baker, and J. L. Gole, ECS Transactions , Vol 69**,** 2, pp. 141–152, 2015. ECS by permission.

In an alternate and important approach, Barillaro et al. [72,73] have demonstrated linearity by integrating PSi sensors with electronic circuits fabricated on the same chip. This method can be applied in using the current selected pore configuration.

In order to evaluate the micron pore decorated PSi hysteresis, the IV response associated with the sensor substrates has been tested for linearity and bias. Figure 14 below shows the IV curves obtained for an operating sensor depicted schematically in Figure 1.Forward and reverse scans for recently produced sensors feature linearity over the entire testing range as well as displaying zero bias. Based on the near linear IV curve, the continuous power consumption is between 25 and 60 microwatts/second over the range 1 to 1.5 volts.

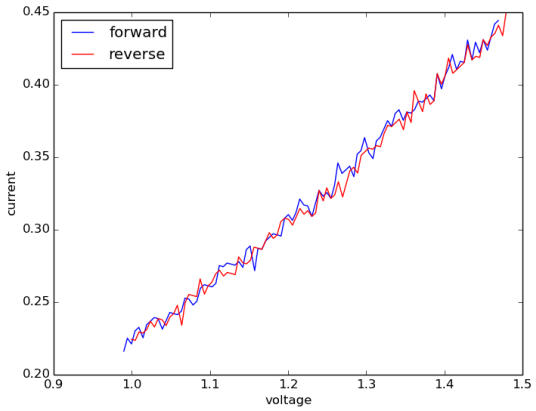

Figure 14. IV (product of current and voltage) curves for continuous sensor response [34]. Elsevier by permission.

5. Time varying operation and false positive sensing in an unsaturated mode

In order to further improve the sensitivity and stability of porous silicon sensors, one can apply pulsed system frequency analysis (PSFA) in which methods of acoustic theory are applied to signal analysis. The benefits of this approach include improved measurement sensitivity, isolation of periodic noise sources, and the ability to evaluate the trade-off between the precision and duration of measurement. This further aids the design of an experimental system. A defined gas pulsing technique is combined with FFT signal analysis to allow a sensor gas response to be measured, without saturation, and filtered on a drifting baseline, so as to eliminate false positives and the effects of external noise (as might be associated with pressure, temperature, and humidity variation) [19]. Figure 15 depicts a test in which the concentration of ammonia (in N_2) being delivered to a sensor was pulsed between 0 and 5 ppm at a frequency of 1/60s (0.017 Hz). The baseline for the device increases during the test as the adsorption and desorption of ammonia begin to equilibrate. However, the magnitude of the signal at the beginning and end of the pulsing sequence and throughout the sequence remains virtually the same as one operates in an unsaturated mode. The sensor baseline can also be affected by low frequency changes in temperature and pressure, however, by introducing a pulsed mode of operation to the sensor systems, this drift can be both "locked out" and monitored [19]. In introducing an FFT analysis to the reversibly, linearly responding, PSi gas sensor, the gas response can be acquired and filtered on a drifting baseline or in the presence of external noise sources (Figures 16, 17).

Figure 16 depicts an example of the raw data and the high fidelity outputs after FFT analysis and filtering with the PSFA technique. The benefits of this approach include improved measurement sensitivity and isolation of periodic noise sources. This technique, coupled with the advantages of PSi verses other sensors, does not require stability in the baseline resistance or low thermal sensitivity as thermal noise, random fluctuations, and long settling times are mitigated. Additional benefits include the ability to detect gas signals when environmental signals are dominant, and a greatly reduced testing. The FFT data analysis method for the PSi gas sensor also offers the ability to operate below saturation and provides several safeguards against false positives. If the false positive is associated with the delivered gas, attributes of the "time-delay" module become unstable and the dataset can be withdrawn [19].

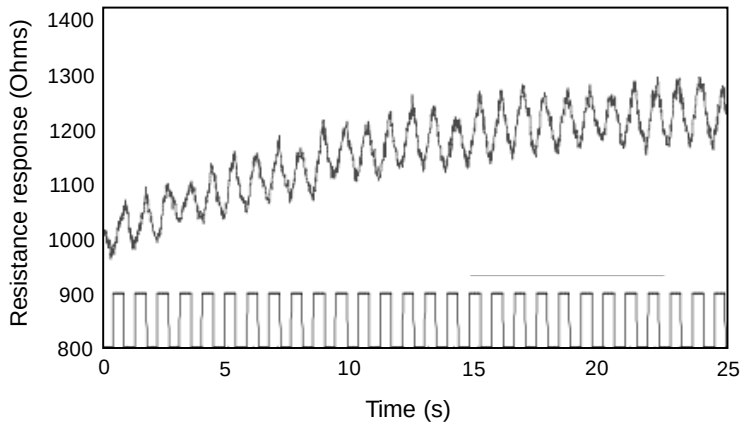

Figure 15. Porous silicon (PSi) sensor response with pulsing of ammonia between 0 and 5 ppm (bottom of figure) in research grade N_2. Note the rise of the baseline, leveling to a plateau as a function of time. The fast Fourier transform technique (FFT, Figures 16, 17) deals with this problem [48].

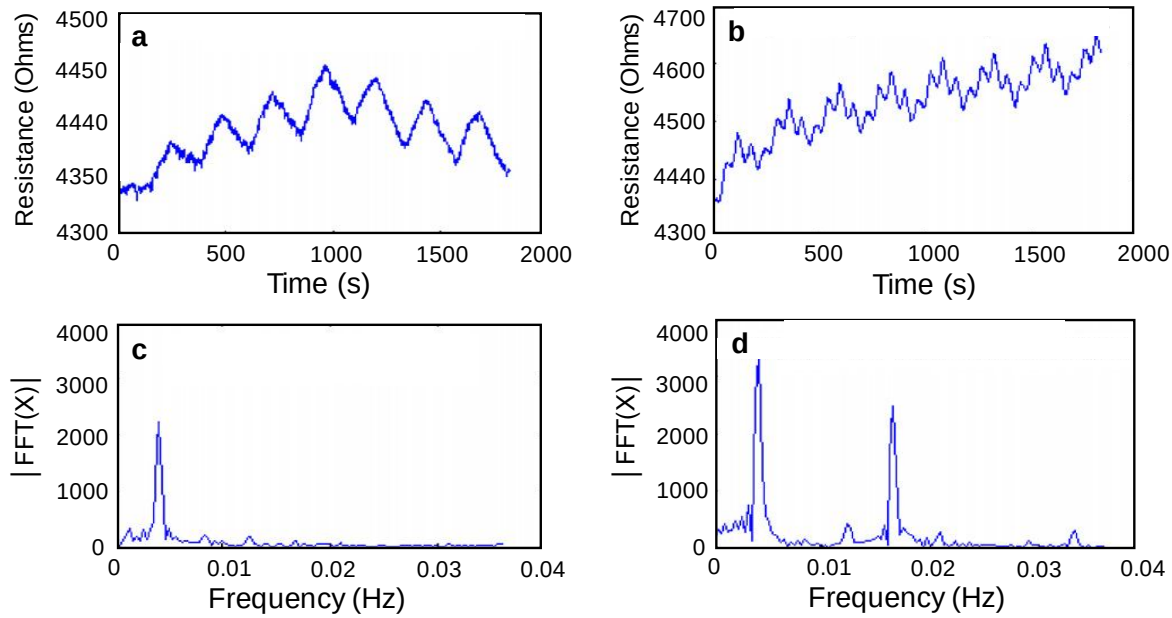

Figure 16. The FFT analysis of a gas pulsing experiment first performed on a sensor ((a) and (c) top and bottom left) whose temperature is varied. The same sensor ((b) and (d) top and bottom right) responding to the same external temperature noise as the sensor is treated with pulsing ammonia (Figure 15). The raw signal of the sensor is shown (top) as well as the filtered FFT of the sensor response (bottom). Separate peaks are generated at an ammonia gas pulsing frequency of 0.0167 Hz and a heating frequency of 0.0042 Hz [19].

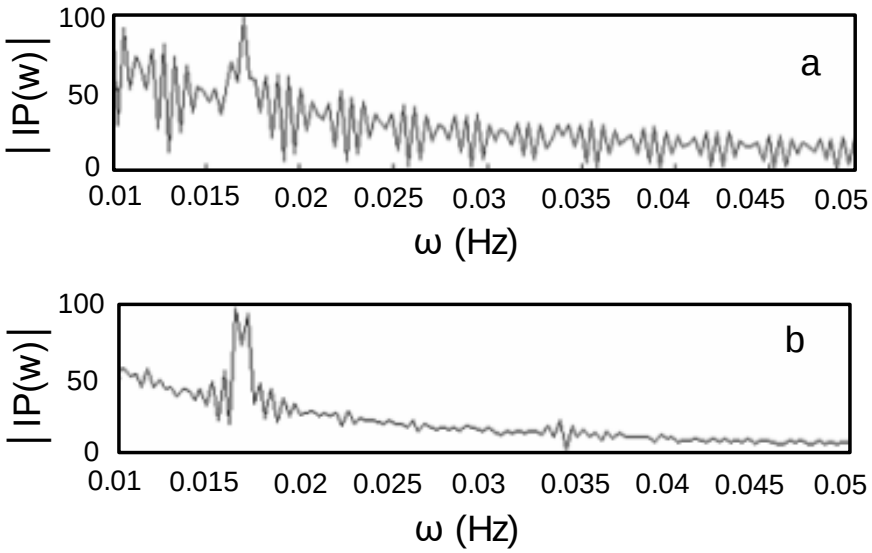

Figure 17. FFT of a PSi gas response before filtering and after filtering [18].

6. Pore diameter selectivity

6.1. Selectivity in multi-gas configurations

A 700–1500 nm diameter PSi pore structure facilitates minimal interaction with water vapor. Similarly, micrometer sized pores would appear to play a dominant role in minimizing interaction

with organic solvents and volatile organic compounds (VOC's) for which the configuration of Figure 1 is hardly sensitive. A general platform for the sensitive and selective detection of the inorganic pollutants H_2S, SO_2, NO, NO_2, and NH_3 on micron pored PSi has demonstrated a vapor phase sensitivity greatly dominating the BTEX contaminants benzene, toluene, and xylene [24]. Sensitivities have been varied using a diversity of nanostructured island sites deposited to the PSi interface. Response ratios well in excess of 10^4:1 for benzene and toluene and 10^3:1 for xylene have been observed, as exemplified for H_2S in Figure 18. The observed responses signal pore diameter selectivity. This selectivity will also hold for multiple gas combinations of the inorganic analytes interacting with the BTEX compounds.

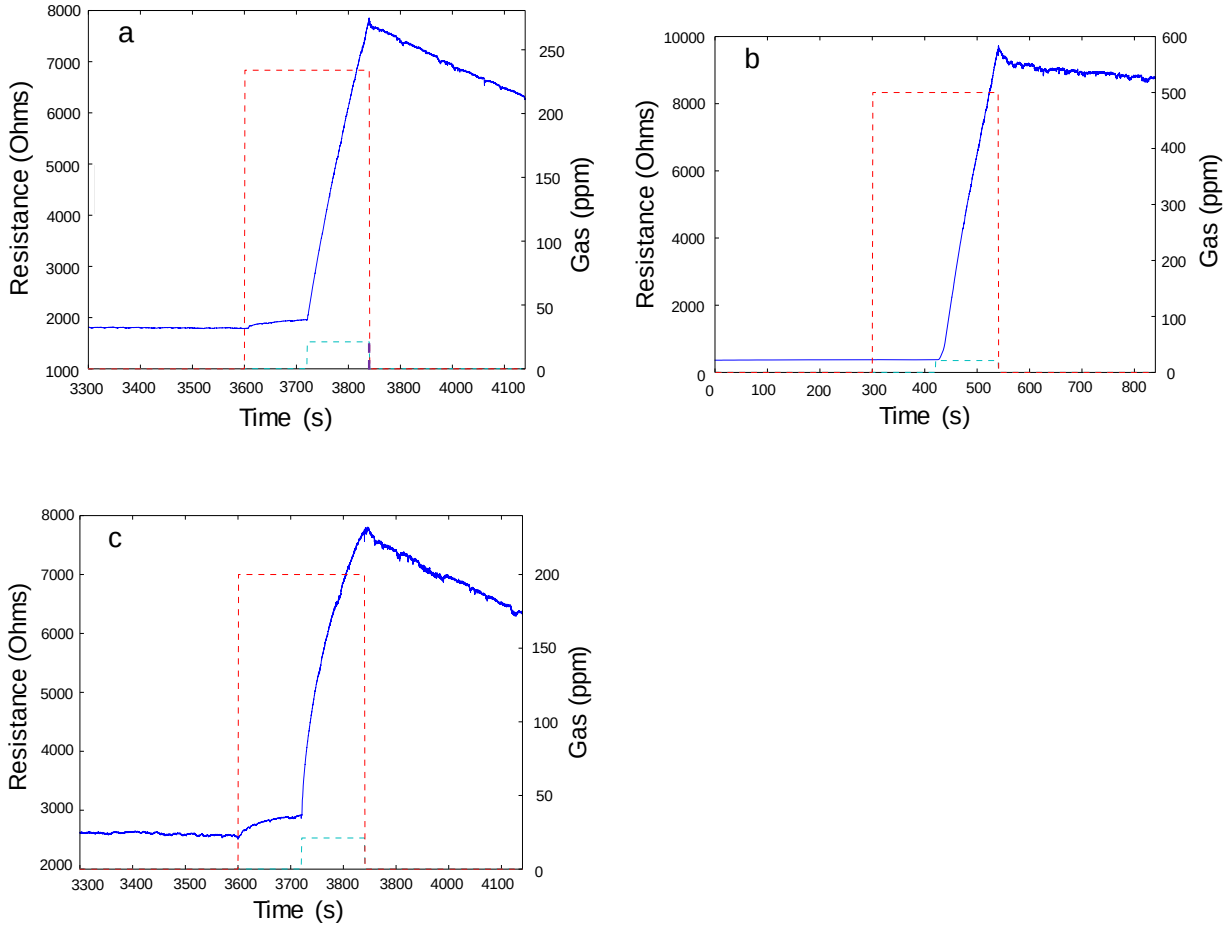

Figure 18. Comparison of relative response for (a) benzene (red box-units right divided by 100) concentrations calculated [23] to be upwards of 20000 ppm, (b) toluene (red box-units right) concentrations in excess of 500 ppm and (c) xylene (red box-units right) concentrations in excess of 200 ppm. The H_2S concentration is 23 ppm over the range denoted by the aqua box for an SnO_x decorated *p*-type PS sensor. Note the relative analyte sensitivity scale. Here H_2S acts as a moderately strong base, donating electrons to p-type PSi and decreasing majority charge carriers. The resistance increases (conductance decreases).

The extension of semiconductor-based devices to multiple-gas sensing is a complex problem. The measurement of two gases simultaneously can be approached with an array-based format by

combining the matrices of nanostructured island site responses for the considered gases, the distinctly different responses of p and n-type interfaces, and the time dependence of these observed responses. Using this approach, one can consider a mixture of amphoteric NO and the moderate acid NO_2 (see Tables 1, 2). NO_2 on interaction with a p-type interface shows an increased conductance whereas it demonstrates an increased resistance for an n-type interface. NO shows an increased resistance for both p and n-type interfaces. Note also that NO and NO_2 have very different nanostructured island site responses, sensitivities, and adsorption constants. The moderate base, NH_3, displays an increasing resistance for a p-type interface and an increasing conductance for an n-type interface and nanostructured island site sensitivities distinct from both NO and NO_2. These differences can be used to approach gas separation.

An initial modeling of the sensor interface for distinct metal oxide nanostructure deposited interfaces is depicted in Figure 19 [20].The exemplified experimental data was taken by measuring the conductometric response to NO and NH_3 for an undecorated PS sensor interface followed by two nanostructured metal oxide decorated PS interfaces. This data was then fit using equations for the two gases based on the Langmuir absorption isotherm [20]. When measuring multiple gases, as demonstrated in Figure 19, it is important to note that the NO and the NH_3 responses on p-type silicon do not add together. This nonlinearity of the response must be understood in order to analyze multiple gases simultaneously [20]. Although the gas responses do not add together linearly, the multi-gas response is repeatable and independent of any initial gas on the surface. This independence has been demonstrated by the similar responses of the gas sensors to an NH_3/NO mixture.

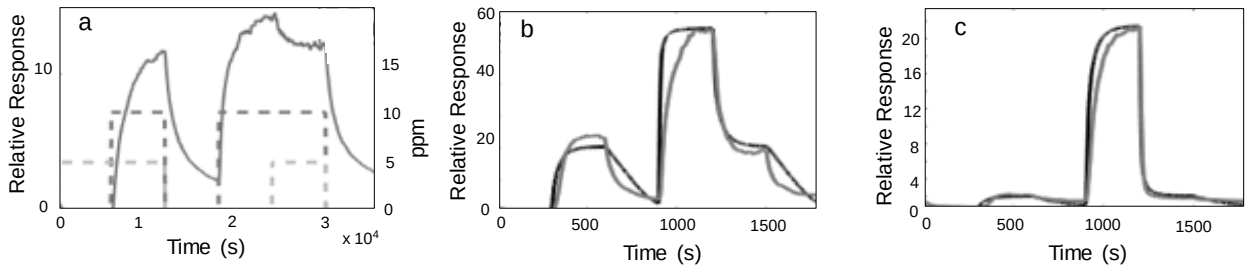

Figure 19. Response (normalized to the baseline resistance) of p-type (a) undecorated (b) PSi/TiO_2 (c) PSi/Au_xO interfaces to 5 ppm of NO (0–300 sec), NH_3 (900–1200 sec) and NO and NH_3 simultaneously (300–600 sec and 1200–1500 sec) compared to a simulated response. For the uncoated interface, the ranges are indicated by black dashes for NH_3 and aqua dashes for NO and the numbers 1–3 correspond to units of 500 s**.** In figures (b) and (c), the simulated Langmuir model in black is compared to the features for the actual data. Similar results are obtained for PSi/MgO, PSi/Ca, and PSi/Ba inter4faces [20]. Note that the response of the mixed gas levels off to a specific value independent of the order in which the gases are exposed to the sensor [20].

The variables of the simulation, the adsorption constants and sensitivities to NH_3 and NO, were calculated from the peak heights of the experimental data. These were translated into appropriate variables using a fitting program. Determined variables for several interfaces are given in Table 4. Data obtained for magnesium oxide was more difficult to fit primarily because of the slow diffusion times of the NH_3 gas into this interface. Normally the gas response begins to saturate after 300 s,

creating a flat line response; however, in this case, the gas diffuses so slowly into the sensor that the system does not saturate over the experimental run time.

The sensitivities reported in Table 4 [20] are completely consistent with the stronger interaction of NH_3 with porous silicon. The adsorption constants, determined from a fit of the Langmuir equation, correspond to the adsorption coefficient divided by the desorption coefficient of NH_3 or NO. The adsorption constants expressed as a measure of the standard free energies of adsorption and desorption are consistent with expected experimental results. For an adsorption constant greater than one, the adsorption process dominates the desorption process. This is the case for NO, which desorbs readily. However, ammonia is a "sticky" gas, which desorbs more slowly than it adsorbs. For all sensors reported in Table 4, the adsorption constant for NH_3 is less than one and is generally much less than that for NO. Calculations show that the adsorption energy from the fitted data is close to 0.05 to 0.15 eV for NO (1.1 to 3.5 kcal/mole) and from 0.02 to 0.05 eV (0.4 to 1.1 kcal/mol) for NH_3. These values are in the range expected for physisorption.

Table 4. Sensitivity (S), adsorption constant (K), and diffusion constant (D) for Diffusion-Adsorption Model of NO and NH_3 interacting with nanostructured metal oxide decorated PSi.

Metal Oxide	Sensitivity		Adsorption constant		Diffusion constant (m^2/s)	
	NO*	NH_3	NO	NH_3	NO	NH_3
Au_xO	-0.27	24.76	14.4	0.47	4.9×10^{-9}	4.9×10^{-9}
TiO_2	-0.73	69.76	0.93	0.41	4.9×10^{-9}	4.9×10^{-9}
CaO	-0.21	0.527	0.21	0.377	4.9×10^{-9}	4.9×10^{-9}
MgO	-0.4	13.78	4.82	0.28	4.9×10^{-12}	4.9×10^{-12}
BaO	-0.7	2.24	0.38	0.12	4.9×10^{-11}	4.9×10^{-11}

*Note: Negative sign indicates that resistance decreases in contact with NO (conductance of interface increases) [20].

While a diffusion-linear interaction model and a diffusion-adsorption model were useful for providing insights into the diffusion and adsorption processes [20,74] of the analyte gas-porous silicon interaction, the fit requires improvement. Figure 20(a) demonstrates a comparison of different saturation response mechanisms to describe the change in response, ΔR, measured experimentally for Au_xO decorated PS interfaces interacting with NH_3. The measured and simulated saturation responses, including a log-log and derivative of the responses are compared for concentrations up to 50 ppm. An inspection of the log-log and derivative of the response demonstrates that the Langmuir adsorption isotherm struggles to fit the experimentally collected values. The Langmuir adsorption isotherm only marginally fits the log-log plot of the data and is non-linear (and vice versa). However, it was found that a developed Fermi distribution function (FDF) [21,23] provides a considerably improved fit to the experimental data for all cases. This diffusion-FDF interaction model suggests that electrical effects dominate adsorption effects [21,23] over the concentration range considered.

A more extended approach is outlined in Figure 21, again for mixed gas analytes. Here, the Inverse Hard/Soft acid /base (IHSAB) concept was used to assess a diversity of conductometric responses for mixed gas interactions, and this framework has been used, in part, to evaluate nonlinear interactions of the analyte gases. Typical interactions described in detail in Ref. 22 are exemplified in

Figure 21. Sensor response to the various analytes depends on the other analytes that are present. This process is dictated by the IHSAB model.as it is used to evaluate compound interactions. An example of the initial mode of analysis is provided in Figure 21 where interacting NH_3 and H_2S influence each other in a manner that can be evaluated. Here, a first analyte response on the sensor must be taken into account to describe a second analyte response. These modifications are well represented using a combination diffusion/absorption- based model for multi-gas interaction that applies the FDF absorption isotherm [21–23]. The coupling of this model with the IHSAB concept describes the considerations in the modeling of a multi-gas mixed analyte-interface, and analyte -analyte interactions. Taking into account the molecular electronic interaction of both the analytes with each other and the extrinsic semiconductor interface, it is possible to demonstrate how the presence of one gas can enhance or diminish the reversible interaction of a second gas with the decorated extrinsic semiconductor interface. The approach begins to illustrate considerations in using array-based formats for multi-gas sensing and its applications.

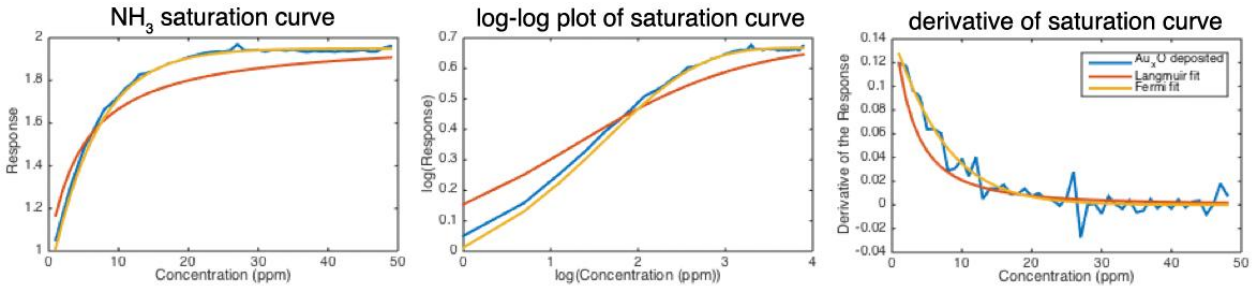

(a)

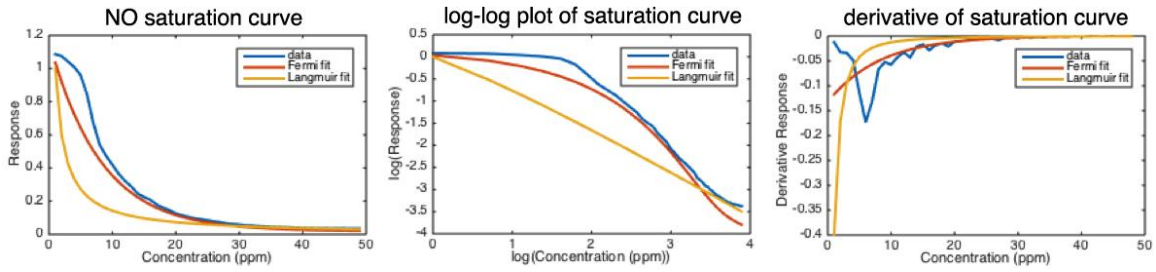

(b)

Figure 20. The saturation response curve (normalized to the baseline resistance) for an Au_xO nanostructure decorated p-type sensor upon exposure to (a) NH_3 and (b) NO concentrations from zero to 50 ppm. Both the experimentally measured sensor response to NH_3 and NO are in blue. For (a) NH_3, the best fits using a Langmuir model are in red and the Fermi distribution function (FDF) fits are in gold. For (b) NO, the Langmuir fits are in orange and the FCF fits are in red. The log-log plot (middle) vs. the log of the concentration (ppm) and the derivative of the saturation response curve (right) again vs. concentration (ppm) illustrate the notably better fit of the FDF model. From W. Laminack, J. L, Gole, ECS Journal of Solid State Science and Technology, 1; 5(2), P80–7, 2016. ECS by permission.

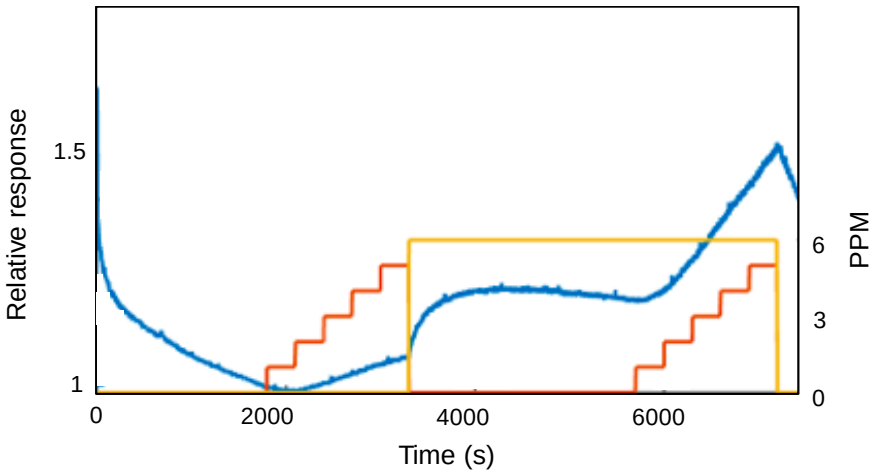

Figure 21. Relative response (normalized to baseline resistance) for an NH_3 saturation curve with H_2S. Au_xO deposited p-type interface response to an NH_3 (red) / H_2S (yellow) mixture. The interface is brought to a base line through treatment with UHP nitrogen for 1800 s. NH_3 is slowly added to the decorated interface in one ppm concentration steps (scale right). Once the initial stepped NH_3 exposure ceases, H_2S (6 ppm) is exposed to the surface and is allowed to equilibrate. The NH_3 is,again, slowly added stepwise to the interface. The response to NH_3 is greater with the H_2S gas as background [22].

The two sensor simulated response for two analyte gases in Figure 22 was modeled using data for SO_2 and PH_3. SO_2 and PH_3 pulsed onto an Au_xO and SnO_x decorated PS surface were evaluated. Using data previously obtained [17,22] a simple response matrix was created. The sensors had equivalent responses to SO_2 and PH_3 before the interface was treated with metal oxide nanoparticles. A tin oxide decorated sensor response increases by a factor of 2 for PH_3 and 4 for SO_2 relative to PSi, while the Au_xO decorated sensor has a response that increases by 5 for PH_3 and 2 for SO_2. This data can be used to create the response matrix [17] given by:

$$M = \begin{bmatrix} S(\mathrm{Au_xO}, \mathrm{SO_2}) & S(\mathrm{Au_xO}, \mathrm{PH_3}) \\ S(\mathrm{SnO_2}, \mathrm{SO_2}) & S(\mathrm{SnO_2}, \mathrm{PH_3}) \end{bmatrix} = \begin{bmatrix} 4 & 2 \\ 2 & 5 \end{bmatrix}$$

where $S(\text{metal oxide}, \text{analyte})$ represents the factor by which the sensor response increases after metal oxide nanostructure deposition for 1 ppm of analyte gas.

From the response matrix derived from experimental data, the optimal method for extracting the concentration (from the simulation) involves taking a second derivative of the data and then multiplying the derivatives with the inverted response matrix for the gas sensor response. Once the responses are calibrated, it is possible to accurately extract the concentration from the simulated data.

While the evaluation in Figure 22 is encouraging, a problem that must be confronted is that of noise and fluctuations. The problem might be handled with a dynamical approach (non-linear correlated noise). A "zeroth order" model (linear) similar to that in Figure 22 could be used to obtain a quantitative idea of the size of the interaction/correlation effects. Subsequently, a modified "first-order" dynamical model of the experimental data could embody non-linear interactions, the advantage being that the inclusion of fluctuations can readily be accomplished. This must await further study.

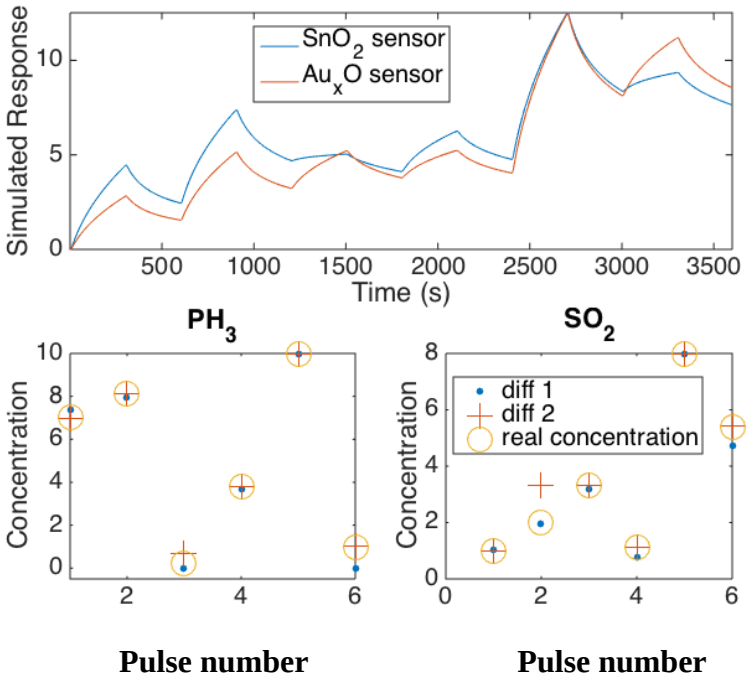

Figure 22. Extracted gas concentrations from a simulated response (normalized to undecorated PSi). Gas simulations of two sensors without any noise are presented at the top. The extracted concentration versus the actual concentration is seen at the bottom of the figure for the two simulated gases. Diff 1 represents the extracted concentration using only the first derivative while Diff 2 represents the extracted concentration using the second derivative [23]. From W. Laminack, J. L, Gole, .ECS Journal of Solid State Science and Technology, 1; 5(2), P80–87, 2016. ECS by permission.

7. Summary and conclusion

We have commented on and reviewed the importance of select nanostructure metal oxide decorated micrometric pore generation in approaching the use of porous silicon (PSi) as a sensitive sensor interface which minimizes interaction with water vapor. Further, we have emphasized the importance of direct *in-situ* nitridation as a means of preparing a hydrophobic interface as demonstrated for $TiO_{2-x}N_x$ nanostructures. The micrometric pore structure and direct nitridation provide a means of greatly enhancing the stability of a PSi sensor as demonstrated in studies of SiO_xNy thin films. This enhanced stability also benefits system linearity and provides a notable improvement of. hysteresis effects. Approaches to sensor selectivity are outlined and considered.

Acknowledgements

It is a pleasure to acknowledge helpful discussions with Professor Kurt Wiesenfeld and Dr. William Laminack. Special thanks go to Dr. Monica Vasiliu and Professor David Dixon for their help in preparing the figures for this manuscript. This Review has no external funding.

Conflict of interest

The author declares that there is no conflict of interest with this review.

References

1. Korotcenkov G, Rusu E (2019) How to Improve the Performance of Porous Silicon-Based Gas and Vapour Sensors? Approaches and Achievements. *Physica Status Solidi (A)* 216: 190348.
2. Korotcenkov G (2010) Chemical Sensors: Fundamentals of Sensing Materials, Volumes 1–3. Momentum Press, New York.
3. Korotcenkov G (2013) Handbook of Gas Sensor Materials, Volumes 1–2. Springer, New York.
4. Canham L (1998) Properties of Porous Silicon. INSPEC, London.
5. Canham L (2014) Handbook of Porous Silicon. Springer, Zug Heidelberg, Switzerland.
6. Korotcenkov G (2015) Porous Silicon: From Formation to Application, Formation and Properties, Volume One. Taylor and Frances Group, CRC Press, Boca Raton.
7. Korotcenkov G (2015) Porous Silicon: From Formation to Application: Biomedical and Sensor Applications, Volume Two. Taylor and Frances Group, CRC Press, Boca Raton.
8. Feng ZC, Tsu R (1994) Porous Silicon. World Science, Singapore.
9. Lehmann V (2002) Electrochemistry of Silicon: Instrumentation, Science, Materials, and Applications. Wiley-VCH Verlag Gmbh, Weinham.
10. Sailor MJ (2012) Porous Silicon in Practice. Wiley-VCH Verlag Gmbh, Weinham.
11. Mares JJ, Kristofik J, Hulcius E (1995) Influence of humidity on transport in porous silicon. *Thin Solid Films* 255: 272–275.
12. Connolly EJ, Timmer B, Pham HTM, et al. (2005) A porous SiC ammonia sensor. *Sensor Actuat B-Chem* 109: 44–46.
13. Fuejes PJ, Kovacs A, Duecso Cs, et al. (2003) Porous silicon-based humidity sensor with interdigital electrodes and internal heaters. *Sensor Actuat B-Chem* 95: 140–144.
14. Korotcenkov G, Cho BK (2010) Porous semiconductors: advanced material for gas sensor applications. *Crit Rev Solid State* 35: 1–37.
15. Wang Y, Park S, Yeow JTW, et al. (2010) A capacitive humidity sensor based on ordered macroporous silicon with thin film surface coating. *Sensor Actuat B-Chem* 149: 136–142.
16. Foell H, Christopherson M, Carstensen J, et al. (2002) Formation and application of porous silicon. *Mater Sci Eng R* 39: 93–141.
17. Gole JL, Laminack W (2010) General approach to design and modling of nanostructure modified semiconductor and nanowire interfaces for sensor and microreactor applications. In: *Chemical Sensors: Simulation and Modeling*, Solid State Sensors, Korotcenkov G. (Ed.) Momentum Press, New York, 87–136.
18. Gole JL, Fedorov AG, Hesketh P, et al. (2004) Phys Status Solidi, C 1(S2): S188–197. Wiley by permission. Copyright © 2004 WILEY-VCH Verlag GmbH & Co. KGaA, Weinheim.
19. Lewis SE, DeBoer JR, Gole JL (2007) Pulsed system frequency analysis for device characterization and experimental design: Application to Porous Silicon Sensors and Extension. *Sensor Actuat B-Chem* 122: 20–29.
20. Laminack W, Hardy N, Baker C, et al. (2015) Approach to multi-gas sensing and modeling on nanostructure decorated porous silicon substrates. *IEEE Sensors* 15: 6491–6497.

21. Laminack W, Baker C, Gole JL (2015) Response simulation and extraction of gas concentrations for nanostructure directed nano/microporous silicon interfaces. *ECS Trans* 69: 141–152.
22. Laminack W, Gole JL (2015) Multi-gas interaction modeling on decorated semiconductor interfaces: a Fermi distribution-based isotherm and the IHSAB principle. *Appl Surf Sci* 359: 774–781.
23. Laminack W, Gole JL (2016) Development of a Fermi energy distribution-based adsorption isotherm on nanostructure decorated porous substrates. *ECS J Solid State Sc* 5: 80–87.
24. Baker C, Laminack W, Gole JL (2016) Selective detection of inorganics NOx, SO_2, and H_2S in the presence of volatile BTEX contaminants toluene, benzene, and xylene. *Air Qual Atmos Health* 9: 411–419.
25. Baker C, Ozdemir S, Gole JL (2016) Nanostructure directed detection of acidic SO_2 and its transformation to basic character. *J Electrochem Soc* 163: B76–B82.
26. Gole JL, Goude EC, Laminack W (2012) Nanostructure driven analyte-interface electron transduction: a general approach to sensor and microreactor design. *Chem Phys Chem* 13: 549–561.
27. Ozdemir S, Osburn T, Gole JL (2011) A nanostructure modifiedporous silicon detection matrix for NO with demonstration of transient conversion of NO to NO_2. *J Electrochem Soc* 158: J201–J207.
28. Laminack W, Pouse N, Gole JL (2012) The dynamic interaction of NO_2 with a nanostructure modified porous silicon matrix: the competition for donor level electrons. *ECS J Solid State Sc* 1: Q25–Q34.
29. Laminack W, Gole JL (2013) Nanostructure directed chemical sensing: the IHSAB principle and the effect of nitrogen and functionalization on metal oxide decorated interface response. *Nanomaterials* 3: 469–485.
30. Baker C, Laminack W, Gole JL (2015) Sensitive and selective detection of H_2S and application in the presence of toluene, benzene, and xylene. *Sensor Actuat B-Chem* 212: 28–34.
31. Laminack W, Baker C, Gole JL (2016) Air quality and the selective detection of ammonia in the presence of toluene, benzene, and xylene. *Air Qual Atmos Health* 9: 231–239.
32. Gole JL, Ozdemir SA (2010) Nanostructure directed physisorption vs. chemisorption at semiconductor interfaces: the inverse of the hard-soft acid-base concept. *ChemPhysChem* 11: 2573–2581.
33. Laminack W, Baker C, Gole JL (2015) Sulphur-Hz(CHx)y(z=0,1) functionalized metal oxide nanostructure decorated interfaces: evidence of Lewis base and Bronsted acid sites- influence on chemical sensing. *Mater Chem Phys* 160: 20–31.
34. Gole JL (2015) Increasing energy efficiency and sensitivity with simple sensor platforms. *Talanta* 132: 87–95.
35. Barsan N, Schweizer-Berberich M, Göpel W (1999) Fundamental and practical aspects in the design of nanoscaled SnO_2 gas sensors: a status report. *Fresenius Journal of Analytical Chemistry* 365: 287–304.
36. Comini E (2006) Metal oxide nano-crystal for gas sensing. *Anal Chim Acta* 568: 28–40.
37. LeGorea LJ, Lada RJ, Moulzolfa SC, et al. (2002) Defects and morphology of tungsten trioxide thin films. *Thin Solid Films* 406: 79–86.

38. Rani S, Roy SC, Bhatnagar M (2006) Effects of Fe doping on the gas sensing properties of nano-crystalline SnO_2 thin films. *Sensor Actuat B-Chem* 122: 204–210.
39. Jiménez I, Arbiol J, Dezanneau G, et al. (2003) Crystal structure, defects and gas sensor response to NO_2 and H_2S of tungsten trioxide nanopowders. *Sensor Actuat B-Chem* 93: 475–485.
40. Moulzolf SC, Ding S, Lad RJ (2001) Stoichiometric and microstructure effects on tungsten oxide chemirestive films. *Sensor Actuat B-Chem* 77: 375–382.
41. Ponce M, Aldao C, Castro M (2003) Influence of particle size on the conductance of SnO_2 thick films. *J Eur Ceram Soc* 23: 2105–2111.
42. Rothschild A, Komem Y (2004) The effect of grain size on the sensitivity of metal oxide gas sensors. *J Appl Phys* 95: 6374–6380.
43. Yoon DH, Choi GM (1997) Microstructure and CO gas sensing properties of porous ZnO produced by starch addition. *Sensor Actuat B-Chem* 45: 251–257.
44. Morrison SR (1987) Selectivity in semiconductor gas sensors. *Sensors and Actuators* 12: 425–440.
45. Watson J (1994) The stannic oxide gas sensor. *Sensor Rev* 14: 20–23.
46. Yamazoe N, Shimiza K, Aswal DK, et al. (2007) Overview of Gas Sensor Technology. Nova Science Publishers Inc., New York.
47. Ozdemir S, Gole JL (2007) The potential of porous silicon gas sensors. *Curr Opin Solid St M* 11: 92–100.
48. Lewis SE, De Boer JR, Gole JL, et al. (2005) Sensitive, selective, and analytical improvements to a porous silicon gas sensor. *Sensor Actuat B-Chem* 110: 54–65.
49. Pearson RG (1990) Hard and soft acids and bases—the evolution of a chemical concept, Coordin Chem Rev 100: 403–425.
50. Pearson RG (1997) Chemical Hardness. John Wiley VCH, Weinheim.
51. Barillaro G, Diligenti A, Nannini A, et al. (2006) Low-concentration NO_2 detection with an adsorption porous silicon FET. *IEEE Sens J* 6: 19–23.
52. Salonen J, Makila E (2018) Thermally carbonized porous silicon and recent applications. *Adv Mater* 30: 1703819.
53. Barotta C, Faglia G, Comini E, et al. (2001) A novel porous silicon sensor for detection of sub-ppm NO_2 concentrations. *Sensor Actuat B-Chem* 77: 62–66.
54. Schechter L, Ben-Chorin M, Kux A (1995) Gas sensing properties of porous silicon. *Anal Chem* 67: 3727–3732.
55. Raghavan D, Gu X, Nguyen T, et al. (2001) Mapping chemically heterogeneous polymer system using selective chemical reaction and tapping mode atomic force microscopy. *Macromolecular Symposia* 167: 297–305.
56. Okorn-Schmidt HF (1999) Characterization of silicon surface preparation processes for advanced gate dielectrics. *IBM J Res Dev* 43: 351–365.
57. Boinovich LB, Elelyanenko AM (2008) Hydrophobic materials and coatings: principles of design, properities, and applications. *Russ Chem Rev* 77: 583–600.
58. Makaryan A, Sedov IV, Mozhaev PS (2016) Current state and prospects of development of technologies for the production of superhydrophobic materials and coatings. *Nanotechnologies in Russia* 11: 679–695.
59. Ponec V, Knor Z, Cerny S (1974) Adsorption on solids. Butterworth and Co., London.

60. Gole JL, Stout J, Burda C, et al. (2004) Highly efficient formation of visible light tunable $TiO_{2-x}N_x$ photocatalysts and their transformation at the nanoscale. *J Phys Chem* 108: 1230–1238.
61. Chen X, Lou Y, Samia ACS, et al. (2005) Formation of oxynitride as the photocatalytic enhancing site in nitrogen-doped titania nanocatalysts: comparison to a commercial nanopowder. *Adv Funct Mater* 15: 41–49.
62. Laminack W, Gole JL (2014) Direct in-situ nitridation of nanostructured metal oxide deposited semiconductor interfaces: tuning the response of reversibly interacting sensor sites. *ChemPhysChem* 15: 2473–2484.
63. Wang J, Mao B, Gole JL, et al. (2010) Visible-light-driven reversible and switchable hydrophilic to hydrophobic surfaces: correlation with photocatalysis. *Nanoscale* 2: 2257–2261.
64. Shi Y, He L, Guang F, et al. (2019) A review: preparation, performance, and applications of silicon oxynitride film. *Micromachines* 10: 552.
65. Yount J, Lenahan P (1993) Bridging nitrogen dangling bond centers and electron trapping in amorphous NH_3-nitrided and reoxidized nitride oxide films. *J Non-Cryst Solids* 164: 1069–1072.
66. Hori T, Naito Y, Iwasaki H, et al. (1986) Interface states and fixed charges in nanometer-range thin nitride oxides prepared by rapid thermal annealing. *IEEE Electr Device L* 7: 669–671.
67. Itakura A, Shimoda M, Kitajima M (2003) Surface stress relaxation in SiO_2 by plasma nitridation and nitrogen distribution in the film. *Appl Surf Sci* 216: 41–45.
68. Herzberg G (1966) Molecular Spectra and Molecular Structure. Vol. III. Electronic Spectra and Electronic Structure of Polyatomic Molecules. By O. Herzberg, D. Van Nostrand and Company, Inc.: Princeton, NJ.
69. Laminack W, Gole JL (2014) A varaiable response phosphine sensing matrix based on nanostructure treated p and n-type porous silicon interfaces. *IEEE Sens J* 14: 2731–2738.
70. Hamilton JD (1994) Time Series Analysis. Princeton University Press, Princeton.
71. Neimark AV, Ravikovitch PI, Vishnyakov A (2000) Adsorption hysteresis in nanopores. *Phys Rev E* 62: R1493–1496.
72. Barillaro G, Bruschi P, Pieri F, et al. (2007) CMOS-compatible fabrication of porous silicon gas sensors and their readout electronics on the same chip. *Phys Status Solidi A* 204: 1423–1428.
73. Barillaro G, Strambini LM (2008) An integrated CMOS sensing chip for NO_2 detection. *Sensor Actuat B-Chem* 134: 585–590.
74. Baker C, Laminack W, Gole JL (2016) Modeling the absorption/desorption response of porous silicon sensors. *J Appl Phys* 119: 124506.